24th International Meshing Roundtable (IMR24)

Defining an $\mathcal{L}_2$-disparity measure to check and improve the geometric accuracy of non-interpolating curved high-order meshes

[a]*Laboratori de Càlcul Numèric (LaCàN), Departament de Matemàtica Aplicada III (MA III), Universitat Politècnica de Catalunya (UPC), Campus Nord UPC, 08034 Barcelona, Spain.*
[b]*Computer Applications in Science and Engineering, Barcelona Supercomputing Center, 08034 Barcelona, Spain.*
Aerospace Computational Design Laboratory, Department of Aeronautics and Astronautics, Massachusetts Institute of Technology, Cambridge, MA 02139, USA.

Abstract

We define an $\mathcal{L}_2$-disparity measure between curved high-order meshes and parameterized manifolds in terms of an $\mathcal{L}_2$ norm. The main application of the proposed definition is to measure and improve the distance between a curved high-order mesh and a target parameterized curve or surface. The approach allows considering meshes with the nodes on top of the curve or surface (interpolative), or floating freely in the physical space (non-interpolative). To compute the disparity measure, the average of the squared point-wise differences is minimized in terms of the nodal coordinates of an auxiliary parametric high-order mesh. To improve the accuracy of approximating the target manifold with a non-interpolating curved high-order mesh, we minimize the square of the disparity measure expressed both in terms of the nodal coordinates of the physical and parametric curved high-order meshes. The proposed objective functions are continuously differentiable and thus, we are able to use minimization algorithms that require the first or the second derivatives of the objective function. Finally, we present several examples that show that the proposed methodology generates high-order approximations of the target manifold with optimal convergence rates for the geometric accuracy even when non-uniform parameterizations of the manifolds are prescribed. Accordingly, we can generate coarse curved high-order meshes significantly more accurate than finer low-order meshes that feature the same resolution.

Peer-review under responsibility of organizing committee of the 24th International Meshing Roundtable (IMR24).

Keywords: High-order mesh, non-interpolative mesh, disparity between manifolds, geometric accuracy, convergence rate

1. Introduction

Unstructured high-order methods have elicited an increasing interest in the community of computational methods since they allow obtaining highly accurate approximations to the solution of a PDE on complex domains, see [1–5]. The approximation obtained with high-order methods converges exponentially with the order of the approximating polynomial when the solution is sufficiently smooth. To enable this exponential converge rate, all these methods rely

* Corresponding author.
E-mail address: xevi.roca@bsc.es

on a curved high-order discretization of the domain which has the potential to accurately approximate the domain. Moreover, the approximation of the geometry with curved meshes reduces the spurious numerical artifacts that may arise from a piecewise linear approximation of the curved domain boundaries [6–11]. To ensure these advantages, it is required that the geometric error is smaller than or comparable to the solution error and therefore, it is mandatory to devise a method to check and reduce the distance between a curved mesh and a target geometry. Otherwise, the geometric error introduced by the high-order mesh may dominate the solution error of the simulation and the theoretical convergence rate may not be achieved.

There are several ways to define a distance between two manifolds, like the Hausdorff distance, the Fréchet distance and the area-based distance and accordingly, different methods to approximate them for practical purposes, see [12–15]. Note that the Fréchet distance and the area-based distance take advantage of the fact that the represented objects correspond to parameterized manifolds. Nevertheless, these useful distance approximations have not yet been proved to allow obtaining high-order curve (surface) mesh approximations that converge exponentially with the order of the approximating polynomial when the target curve (surface) is sufficiently smooth. Moreover, the incorporation of these distances in a continuous minimization process requires one to approximate the derivatives with numerical differentiation schemes that may reduce the quadratic convergence rate of Newton's method.

Taking into account the previous issues, the main contribution of this work is to propose a novel $\mathcal{L}_2$-disparity measure to quantify the deviation between a curved high-order mesh and a parameterized m-dimensional manifold embedded in an n-dimensional space. The main application of the proposed definition is to measure and improve the distance between a non-interpolative curved high-order mesh and a target parameterized curve or surface. We devise the method as follows: first, an auxiliary high-order mesh on the parametric domain is considered with the same topology of the physical curved mesh; second, the auxiliary mesh is lifted to the physical space by using the prescribed parameterization of the target manifold; finally, the $\mathcal{L}_2$ norm of the point-wise difference of the curved mesh and the target manifold determines the disparity measure. Specifically, to obtain the disparity measure the average of the square of the point-wise differences is minimized in terms of the parametric coordinates of the high-order nodes of the auxiliary parametric mesh. Furthermore, to improve the accuracy of approximating the target manifold with a curved high-order mesh, we minimize the square of the disparity measure expressed both in terms of the nodal coordinates of the physical and parametric curved high-order meshes.

All the objective functions introduced in this work are continuously differentiable and thus, we are able to use minimization algorithms that require the exact first or the second derivatives of the objective function. Specifically, in this work we use Newton's method combined with a back-tracking line-search algorithm, see [16]. Note that when minimizing the square of the disparity measure the nodal coordinates are free to move in the physical space and therefore, we obtain a non-interpolative curved high-order mesh that reproduces with optimal accuracy the initial manifold in a weak manner. By allowing a non-interpolative mesh, we are able to obtain a mesh that better approximates the manifold in terms of the proposed $\mathcal{L}_2$-disparity, as we show in one of the examples. The rest of examples illustrate other benefits of the proposed methodology. Specifically, we show that the auxiliary parametric mesh facilitates to obtain high-order meshes that optimally approximate curves defined by non-uniform parameterizations. Furthermore, the proposed methodology provides high-order geometric approximations with optimal convergence rates and therefore, coarse high-order meshes are significantly more accurate than finer low-order meshes.

The rest of the paper is structured as follows. Section 2 reviews the previous work related with this article. Section 3 presents the definition of proposed $\mathcal{L}_2$-disparity measure, and the minimization process to optimize the deviation of a curved high-order mesh and a manifold. Section 4 shows several examples that illustrate the properties of the $\mathcal{L}_2$-disparity measure. Finally, Section 5 presents the conclusions and the future work.

2. Related work

Let Σ_1 and Σ_2 be two m-dimensional manifolds in $\mathbb{R}^n$, parameterized by $\boldsymbol{\varphi}_1$ and $\boldsymbol{\varphi}_2$, respectively, in such a way that

$$\begin{array}{rcl} \boldsymbol{\varphi}_i : \mathcal{U}_i \subset \mathbb{R}^m & \longrightarrow & \Sigma_i \subset \mathbb{R}^n \\ \mathbf{u} & \longmapsto & \mathbf{x} = \boldsymbol{\varphi}_i(\mathbf{u}) \end{array}, \qquad i = 1, 2,$$

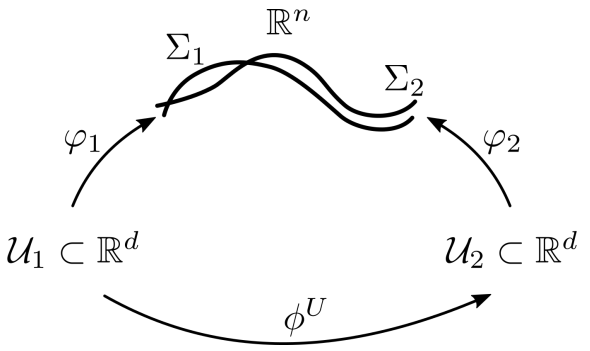

Fig. 1. Two d-dimensional manifolds embedded in $\mathbb{R}^n$, with their respective parameterizations and parametric spaces.

being $\mathcal{U}_1$ and $\mathcal{U}_2$ the parametric spaces of Σ_1 and Σ_2, respectively, see Figure 1. In the literature, there are several manners to compute the distance between them. The Hausdorff distance between Σ_1 and Σ_2 is defined as

$$d_H(\Sigma_1, \Sigma_2) = \max\left\{ \sup_{x\in\Sigma_1} \inf_{y\in\Sigma_2} d(x,y), \sup_{y\in\Sigma_2} \inf_{x\in\Sigma_1} d(x,y) \right\}, \tag{1}$$

being $d(x, y)$ a distance between points. In [12] the authors propose a method to compute the Hausdorff distance between two triangular meshes ($m = 2$, $n = 3$). The main idea is to sample one of the meshes and then compute the closest point of each sample to the other mesh.

Note that the Hausdorff distance is commonly used to compute the distance between two sets. Thus, it does not take into account that Σ_1 and Σ_2 are parameterized manifolds. For this reason, when dealing with manifolds, it is more common to use the Fréchet distance defined as

$$d_F(\Sigma_1, \Sigma_2) = \inf_{\boldsymbol{\phi}^U} \sup_{\mathbf{u}\in\mathcal{U}_1} d(\boldsymbol{\varphi}_1(\mathbf{u}), \boldsymbol{\varphi}_2(\boldsymbol{\phi}^U(\mathbf{u}))), \tag{2}$$

being $\boldsymbol{\phi}^U$ all the possible orientation-preserving diffeomorpisms between $\mathcal{U}_1$ and $\mathcal{U}_2$. It can be proven the d_F is a distance that does not depend on the selected parameterizations for Σ_1 and Σ_2. However, the calculation of d_F is not straightforward, and several approximations to compute it have been proposed. For instance, in [13] the authors compute the Fréchet distance between two polygonal curves ($m = 1$, $n = 2$), and in [14] they compute an approximation of the Fréchet distance between two triangulated surfaces ($m = 2$, $n = 3$).

In [15], the authors define an area-based distance between two polygonal curves in the plane as the area between them. To approximate the area distance between two arbitrary curves ($m = 1$, $n = 2$), they approximate the curves using poly-lines and compute the area distance between the poly-lines. It is important to highlight that the authors use the area-based distance in a minimization process to obtain a high-order mesh that approximates with high accuracy the boundaries of the geometry. In the minimization process, the derivatives of the area-based distance with respect to the nodal coordinates are computed using finite differences, which may reduce the quadratic convergence rate of Newton's method.

In this paper, we define an $\mathcal{L}_2$-disparity measure between two manifolds that is continuously differentiable and, for this reason, can be introduced in a continuous minimization process. In addition, the proposed definition is valid for manifolds of arbitrary dimension. To compute the $\mathcal{L}_2$-disparity between two manifolds, an optimization problem has to be minimized. We directly apply the $\mathcal{L}_2$-disparity measure between manifolds to the generation of non-interpolative curved high-order meshes. Note that in our setup, the nodes of the optimized high-order mesh are not located on the manifold and accordingly, a non-interpolative mesh is generated.

3. Formulation of the problem

Given two m-dimensional manifolds in $\mathbb{R}^n$, Σ_1 and Σ_2, the $\mathcal{L}_2$-disparity of Σ_1 and Σ_2 is defined as

$$d\left(\Sigma_1, \Sigma_2\right) = \inf_{\boldsymbol{\phi}^U} \left\| \boldsymbol{\varphi}_1 - \boldsymbol{\varphi}_2 \circ \boldsymbol{\phi}^U \right\| = \inf_{\boldsymbol{\phi}^U} \sqrt{\int_{U_1} \left\| \boldsymbol{\varphi}_1 - \boldsymbol{\varphi}_2 \circ \boldsymbol{\phi}^U \right\|^2 \, \mathrm{d}\Omega}, \tag{3}$$

where $\|\cdot\|$ is the Euclidean norm, and $\boldsymbol{\phi}^U$ are all the possible orientation-preserving diffeomorphisms between $\mathcal{U}_2$ and $\mathcal{U}_1$.

Note that the definition of the $\mathcal{L}_2$-disparity introduced in (3) is independent of the selected parameterization of Σ_2 because we are taking the infimum over all the possible orientation-preserving diffeomorphisms between $\mathcal{U}_2$ and $\mathcal{U}_1$.

Given a curved high-order mesh and a manifold in the physical space, $\mathcal{M}^P$ and Σ, respectively, our objective is to quantify the disparity of the mesh and the parameterized manifold, and optimize the position of the mesh nodes in order to better approximate the manifold using the high-order mesh. We assume that the manifold Σ is parameterized by a continuously differentiable and invertible mapping (diffeomorphism)

$$\begin{aligned} \boldsymbol{\varphi} : \mathcal{U} \subset \mathbb{R}^m &\longrightarrow \Sigma \subset \mathbb{R}^n \\ \mathbf{u} &\longmapsto \mathbf{x} = \boldsymbol{\varphi}(\mathbf{u}), \end{aligned}$$

where $\mathcal{U}$ is the parametric space of the surface. In this work, we use the OpenCASCADE library [17] to retrieve the parameterization of the surfaces of a CAD model.

To better approximate the target manifold, we use the $\mathcal{L}_2$-disparity of the mesh and the manifold, see Equation (3). We consider that the mesh is defined as a set of elements, and that for each element in the physical space, e^P, there is a master element e^M. Thus, the physical mesh can be defined in terms of an element-wise parameterization $\boldsymbol{\phi}^P$ in such a way that:

$$\begin{aligned} \boldsymbol{\phi}^P|_{\mathrm{e}^M} : \mathrm{e}^M &\longrightarrow \mathrm{e}^P \subset \mathbb{R}^n \\ \boldsymbol{\xi} &\longmapsto \mathbf{x} = \sum_{i=1}^{n_p} \mathbf{x}_i N_i^{\mathbf{x}}(\boldsymbol{\xi}), \end{aligned}$$

being n_p the number of nodes of the high-order element e^P, $\mathbf{x}_i$ the coordinates of the i-th node in the physical space, and $\{N_i^{\mathbf{x}}\}_{i=1,\dots,n_p}$ a Lagrangian basis of polynomial shape functions of degree p. Thus, in order to minimize the disparity between the mesh and the manifold, we define the functional

$$E(\boldsymbol{\phi}^P; \boldsymbol{\phi}^U) = \left\| \boldsymbol{\phi}^P - \boldsymbol{\varphi} \circ \boldsymbol{\phi}^U \right\|^2 = \left(\boldsymbol{\phi}^P - \boldsymbol{\varphi} \circ \boldsymbol{\phi}^U, \boldsymbol{\phi}^P - \boldsymbol{\varphi} \circ \boldsymbol{\phi}^U \right),$$

where $(\cdot, \cdot)$ is a dot product of functions defined as

$$(f, g) = \sum_{\mathrm{e}^M \in \mathcal{M}^M} \int_{\mathrm{e}^M} fg \, \mathrm{d}\boldsymbol{\xi} = \int_{\mathcal{M}^M} fg \, \mathrm{d}\boldsymbol{\xi},$$

being $\mathcal{M}^M$ the master mesh composed of all the reference elements of the physical mesh. Note that $d\left(\mathcal{M}^P, \Sigma\right) = \sqrt{\inf_{\boldsymbol{\phi}^U} E(\boldsymbol{\phi}^P; \boldsymbol{\phi}^U)}$. Since the mapping $\boldsymbol{\phi}^P$ is determined by the position of the mesh nodes, so does the functional E. That is,

$$E(\boldsymbol{\phi}^P; \boldsymbol{\phi}^U) = E(\mathbf{x}_1, \dots, \mathbf{x}_{N_P}; \boldsymbol{\phi}^U),$$

being N_P the number of nodes of the physical high-order mesh. In order to be able to minimize functional E, we take an element-wise polynomial approximation of the diffeomorphism $\boldsymbol{\phi}^U$. That is, $\boldsymbol{\phi}^U|_{\mathrm{e}^M} \approx \boldsymbol{\phi}_h^U|_{\mathrm{e}^M}$ such that

$$\begin{aligned} \boldsymbol{\phi}_h^U|_{\mathrm{e}^M} : \mathrm{e}^M &\longrightarrow \mathrm{e}^U \subset \mathcal{U} \\ \boldsymbol{\xi} &\longmapsto \mathbf{u} = \sum_{i=1}^{n_u} \mathbf{u}_i N_i^{\mathbf{u}}(\boldsymbol{\xi}), \end{aligned}$$

with $\mathcal{U}$ the parametric space of the manifold parameterization, and $\{N_i^{\mathbf{u}}\}_{i=1,\dots,n_u}$ a Lagrangian basis of polynomial shape functions of degree q. The mapping $\boldsymbol{\phi}^U$ characterizes a parametric high-order mesh, $\mathcal{M}^U$, of polynomial degree q in the parametric space of the manifold, and the position of its nodes is $\mathbf{u}_i$, for $i = 1, \dots, N_U$. Note that the polynomial degree of the parametric mesh and the physical mesh can be different and, in general, are not the same. In an intuitive manner, the parametric mesh allows the alignment of the physical mesh with the parameterization of the geometric entity. Thus, although we do not have yet a theoretical setting to select the value of q, it depends on the parameterization of the geometric entity, and the polynomial degree of the physical mesh, p.

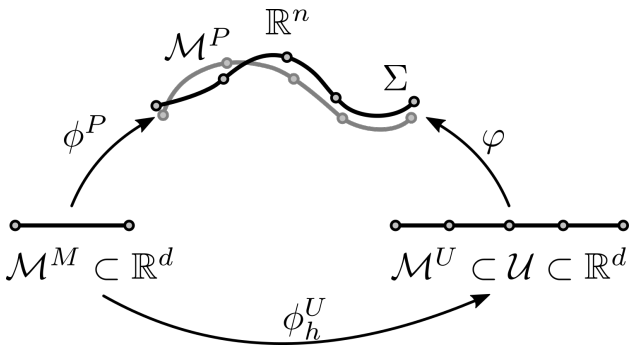

Fig. 2. $\mathcal{L}_2$-disparity measure between a mesh, gray line, and a manifold, black line. To compute the $\mathcal{L}_2$-disparity, an auxiliary parametric mesh, $\mathcal{M}^U$, is used.

Since we approximate $\boldsymbol{\phi}^U$ by $\boldsymbol{\phi}_h^U$, and $\boldsymbol{\phi}_h^U$ is determined by the position of the parametric mesh nodes, $\mathbf{u}_i$, for $i = 1, \ldots, N_U$, functional E is approximated as

$$E(\mathbf{x}_1, \ldots, \mathbf{x}_{N_P}; \boldsymbol{\phi}^U) \simeq E_h(\mathbf{x}_1, \ldots, \mathbf{x}_{N_P}; \boldsymbol{\phi}_h^U) = E_h(\mathbf{x}_1, \ldots, \mathbf{x}_{N_P}; \mathbf{u}_1, \ldots, \mathbf{u}_{N_U}) = \left\| \boldsymbol{\phi}^P - \boldsymbol{\varphi} \circ \boldsymbol{\phi}_h^U \right\|^2 . \tag{4}$$

The minimization of functional E_h with respect to the parametric node coordinates, $\mathbf{u}_i$, for $i = 1, \ldots, N_U$, leads to an approximation of the $\mathcal{L}_2$-disparity between the mesh and the manifold. Moreover, the minimization of functional E_h with respect to the physical node coordinates and the parametric node coordinates, leads to the mesh that *best* approximates the given manifold, Σ, in terms of the proposed $\mathcal{L}_2$-disparity. Note that in this setup, the coordinates of the nodes are not restricted to be on the manifold Σ. That is, we do not seek a mesh that interpolates the manifold. Our aim is to obtain the non-interpolative high-order mesh that *best* approximates the given manifold in a weak sense. Figure 2, shows the used diagram to compute an approximation of the $\mathcal{L}_2$-disparity measure between a curved high-order mesh, $\mathcal{M}^P$, and a manifold, Σ.

In order to minimize Functional (4), it is important to implement a method that features a rapid rate of convergence and global convergence guarantees. To this end, we have applied Newton's method using machine accurate first and second derivatives with a backtracking line search that ensures that Wolfe conditions are fulfilled, see details in [16]. Specifically, the implemented backtracking line-search ensures a sufficient decrease of the objective function and that the curvature conditions are fulfilled. Accordingly, the method has global convergence guarantees as referred in [16]. That is, the norm of objective function gradient converges to zero. Note that it is not ensured that the method converges to a minimizer, but it is guaranteed to be attracted by stationary points. Nevertheless, in general terms, for line search methods, this is the strongest global convergence result that can be obtained. It is important to point out that in all the checked examples this implementation has converged to a physical curved high-order mesh that provides geometric accuracy with the expected rate of convergence.

4. Examples

In this section, we present several examples that show the applicability of the proposed $\mathcal{L}_2$-disparity. The first example illustrates that non-interpolative meshes can be more accurate than interpolative meshes. The next two examples deal with the approximation of one-dimensional curves ($m = 1$) immersed in a two-dimensional space ($n = 2$). For each of them, we show an initial interpolating mesh, and the corresponding smoothed approximating mesh. In both cases, the curves are parameterized with non-uniform length of the tangent vector. Nevertheless, we also present the results of a convergence rate (cr) analysis of the $\mathcal{L}_2$-disparity between the interpolating initial meshes and the curve, and the smoothed approximating meshes and the curve. Finally, in order to show that the proposed $\mathcal{L}_2$-disparity is able to deal with two-dimensional manifolds, the third example shows a mesh that approximates a surface (m=2) in a three-dimensional space (n=3). The example also illustrates that for the same resolution, coarse high-order meshes can be significantly more accurate than fine low-order meshes.

(a) (b)

Fig. 3. Mesh of polynomial degree one (gray line) for the circular arc (black line). $\mathcal{L}_2$-disparity computed using $q = 2$. (a) Initial interpolating mesh ($d = 0.156$); and (b) optimized approximating mesh ($d = 0.065$).

4.1. Non-interpolative but more accurate meshes: a circular arc

In this example, we compare the accuracy of an interpolative linear mesh and a non-interpolative mesh for a circular arc. The $\mathcal{L}_2$-disparity between the linear mesh, Figure 3(a), and the arc is $d\left(\mathcal{M}^0, \Sigma\right) = 1.5 \cdot 10^{-1}$. The $\mathcal{L}_2$-disparity is computed using $q = 2$. By minimizing Functional (4) with respect the physical and parametric nodal coordinates, we obtain a non-interpolative linear mesh, $\mathcal{M}^1$, that better represents Σ in terms of the proposed $\mathcal{L}_2$-disparity, see Figure 3(b). In this case, $d\left(\mathcal{M}^1, \Sigma\right) = 6.5 \cdot 10^{-2}$. This shows that with the proposed approach, we are able to generate a mesh that better approximates the curve, even when the nodes are not located on the circular arc. Hence, the non-interpolative mesh is closer to the circular arc than the initial interpolative mesh.

4.2. Independence on the parameterization: non-uniform parameterization of a circular arc

The objective of this example is to show that the proposed formulation is independent of the selected parameterization of the geometric entity. To this end, we generate a non-interpolative high-order mesh on a circular arc parameterized as follows:

$$\boldsymbol{\varphi}(t) = \left(\cos\left(\pi t^2\right) \, , \, \sin\left(\pi t^2\right) \right), \qquad t \in [0, 1]. \tag{5}$$

Note that this parameterization of the circular arc does not lead to a uniform norm of the tangent vector. We generate a high-order mesh of polynomial degree three with equal-sized elements in the parametric space of the curve, $\mathcal{M}^0$. Note that this induces a mesh in the physical space with elements that are not of the same size, see Figure 4(a). The nodes of the high-order mesh are placed on the curve and therefore, this is an interpolating mesh. It is worth to notice that the initial mesh does not correctly represent the curve. The $\mathcal{L}_2$-disparity between the initial mesh and the curve is $d\left(\mathcal{M}^0, \Sigma\right) = 8.8 \cdot 10^{-2}$. Figure 4(b) shows the smoothed approximating high-order mesh, $\mathcal{M}^1$, obtained after minimizing the functional in Equation (4). Note that we obtain a high-order mesh in which the nodes are not placed on the curve. However, the smoothed mesh better approximates the initial curve, since $d\left(\mathcal{M}^1, \Sigma\right) = 1.7 \cdot 10^{-3}$. Furthermore, the physical nodes are evenly spaced despite the non-uniform parameterization of the circular arc. Figures 4(c) and 4(d) shows the initial and smoothed auxiliary parametric meshes, respectively. Note that the initial parametric mesh is equi-distributed in the parametric space, while the smoothed one is non-uniform. Nevertheless, the physical optimized mesh is composed of uniform elements. Hence, we show that the proposed formulation is independent of the selected parameterization for the circular arc.

Figure 5 presents a convergence rate analysis of the $\mathcal{L}_2$-disparity in an h-refinement process for polynomial degrees between one and four. For each calculation, we use $q = p+8$. Note that the expected convergence rate for a high-order mesh of polynomial degree p is $p + 1$. The initial interpolating meshes achieve a sub-optimal convergence rate of $p + 0.5$. The main reason is that the circular arc is not described using a parameterization with a uniform length of the tangent vector. In the case of the smoothed approximating meshes we obtain a sub-optimal convergence rate in the case of polynomial degree one, and a super-convergence rate in the cases of polynomial degree two, three and four.

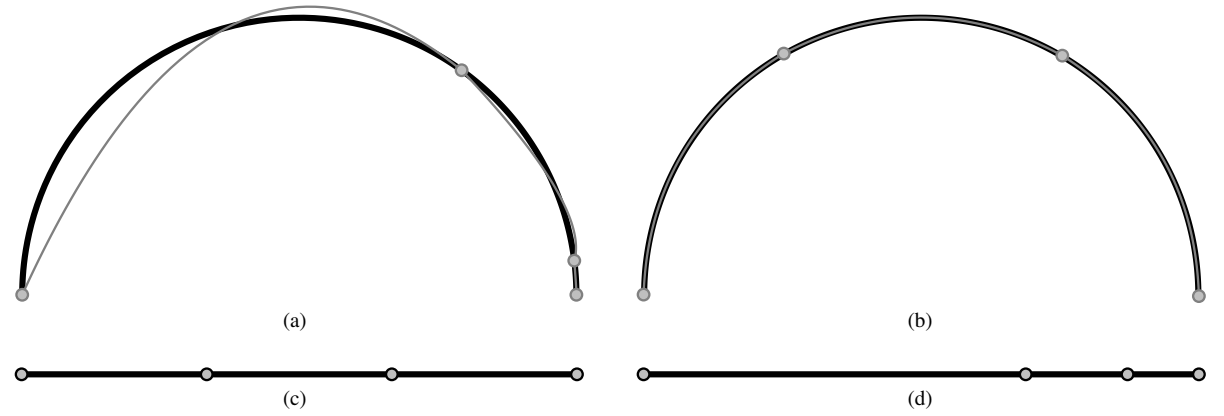

Fig. 4. Mesh of polynomial degree two (gray line) for the re-parameterized circular arc (black line). $\mathcal{L}_2$-disparity computed using $q = 18$. (a) Initial interpolating mesh ($d = 8.8 \cdot 10^{-2}$); (b) smoothed approximating mesh ($d = 1.7 \cdot 10^{-3}$); (c) initial equi-distributed mesh in the parametric space; and (c) final mesh in the parametric space.

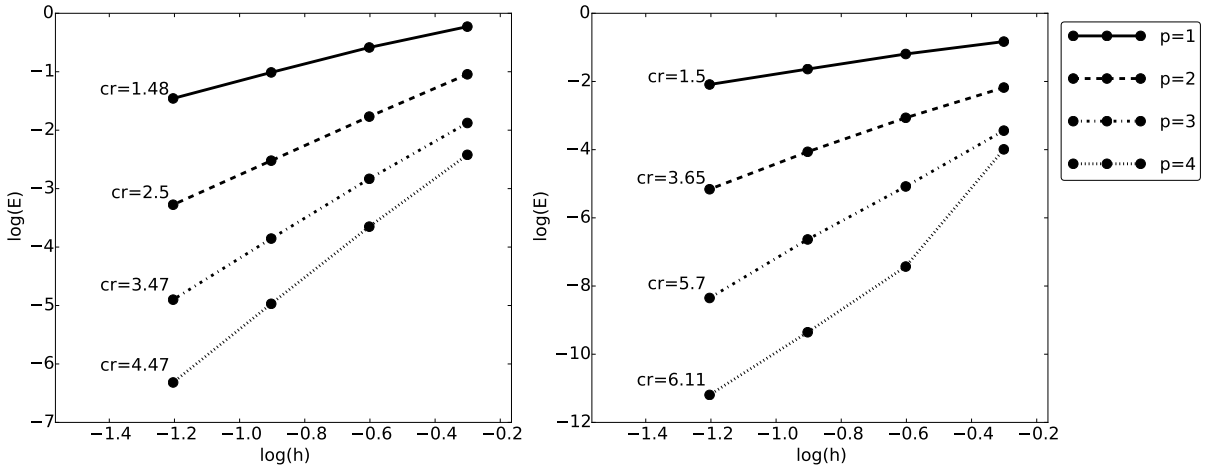

Fig. 5. Convergence rate of the $\mathcal{L}_2$-disparity of the meshes generated for the re-parameterized circular arc using the initial interpolating meshes (left); and smoothed approximating meshes (right). In each case, $q = p + 8$.

4.3. Optimal convergence rate: NACA0012 airfoil curve

This example deals with the generation of a high-order mesh for a NACA0012 airfoil. We generate an interpolative mesh, $\mathcal{M}^0$, of polynomial degree three on the curve, see Figure 6(a). Note that the mesh does not correctly represent the NACA0012 geometry because it contains a sharp corner at the leading edge of the airfoil. The $\mathcal{L}_2$-disparity between the initial mesh and the curve is $d\left(\mathcal{M}^0, \Sigma\right) = 2.1 \cdot 10^{-2}$. After minimizing the functional in Equation (4), we obtain a non-interpolative high-order mesh, $\mathcal{M}^1$, that correctly represents the NACA0012 airfoil. In this case, $d\left(\mathcal{M}^1, \Sigma\right) = 2.3 \cdot 10^{-5}$. Note that we have improved the geometric accuracy of the mesh by three orders of magnitude. In order to obtain a closed mesh, we have imposed periodic boundary conditions when minimizing Functional (4). That is, the we consider that the degrees of freedom associated with the first and last nodes are the same.

Figure 7 presents a convergence rate analysis of the $\mathcal{L}_2$-disparity in an h-refinement process for polynomial degrees between one and four. To compute the $\mathcal{L}_2$-disparity and perform the optimization process, we have used $q = p + 3$, being p the polynomial degree of the mesh. In this case, the initial interpolating meshes do not achieve an optimal convergence rate. Although the accuracy of the meshes increases as the interpolating degree increases, the convergence rate does not increase. The main reason is that these meshes do not correctly approximate the leading edge of

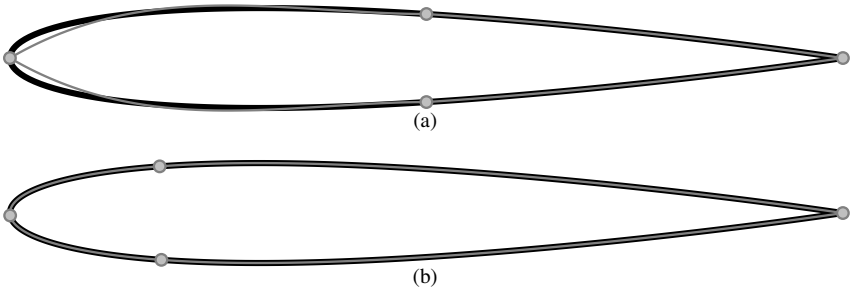

Fig. 6. Mesh of polynomial degree three (gray line) for the NACA0012 airfoil (black line). $\mathcal{L}_2$-disparity computed using $q = 4$. (a) Initial interpolating mesh ($d = 2.1 \cdot 10^{-2}$); and (b) smoothed approximating mesh ($d = 2.3 \cdot 10^{-5}$).

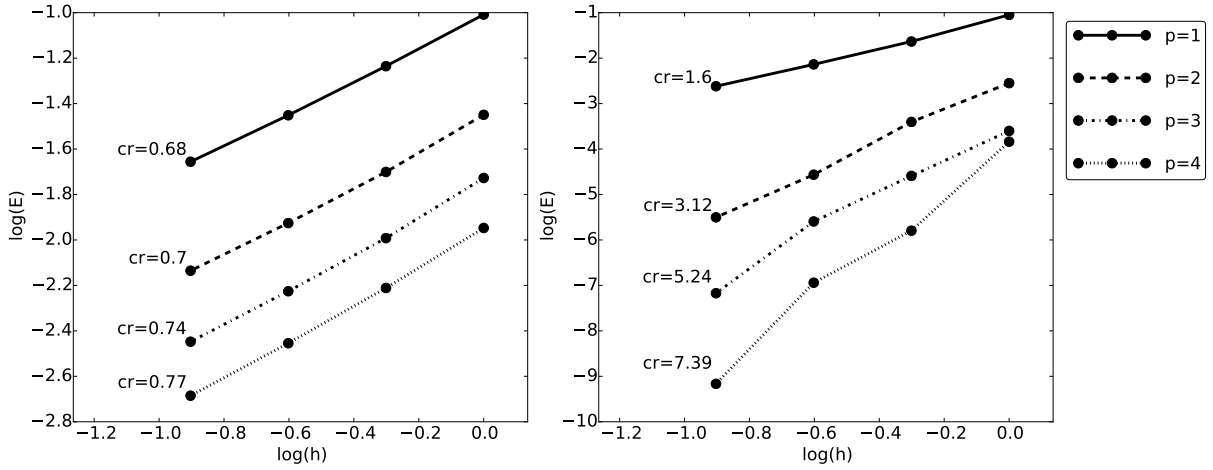

Fig. 7. Convergence rate (cr) of the $\mathcal{L}_2$-disparity of the meshes generated for the NACA0012 using the initial interpolating meshes (left), and smoothed approximating meshes (right). In each case, $q = p + 3$.

the NACA0012, as seen in Figure 6(a). The non-interpolative meshes obtained by minimizing Functional (4) achieve a sub-optimal convergence rate for polynomial degree one. However, the meshes obtained for polynomial degrees between two and four achieve a super-convergence rate.

4.4. Non-constant curvature surface: torus

This example is devoted to show that the proposed formulation can also be applied to curved high-order meshes for surfaces. In order to properly visualize the results, we introduce the point-wise distance between a high-order mesh and a surface as the orthogonal projection of each point of the mesh to the manifold. That is,

$$d(\boldsymbol{\xi}) = d\Big(\boldsymbol{\phi}^P(\boldsymbol{\xi}), \Sigma\Big) = \inf_{\mathbf{u}\in\mathcal{U}} \left\| \boldsymbol{\phi}^P(\boldsymbol{\xi}) - \boldsymbol{\varphi}(\mathbf{u}) \right\|. \tag{6}$$

Note that $\sup_{\boldsymbol{\xi}\in\mathcal{M}^M} d(\boldsymbol{\xi})$ is the one way Hausdorff distance of the mesh and the manifold and, for this reason, it is an upper bound of the Hausdorff distance between the mesh and the manifold. It is important to point out that we do not use the point-wise distance in our formulation. In order to minimize the $\mathcal{L}_2$-disparity between the curved high order mesh and the manifold, we minimize Functional (4). We use the point-wise distance, Equation (6), solely for visualization purposes. Figure 8(a), shows the initial interpolating mesh of polynomial degree six for the torus. The $\mathcal{L}_2$-disparity between the manifold and the initial mesh is $d\left(\mathcal{M}^0, \Sigma\right) = 7 \cdot 10^{-8}$. When we minimize Functional (4), we obtain a non-interpolative mesh, $\mathcal{M}^1$, that represents with higher accuracy the geometry, see Figure 8(b). Specifically, the

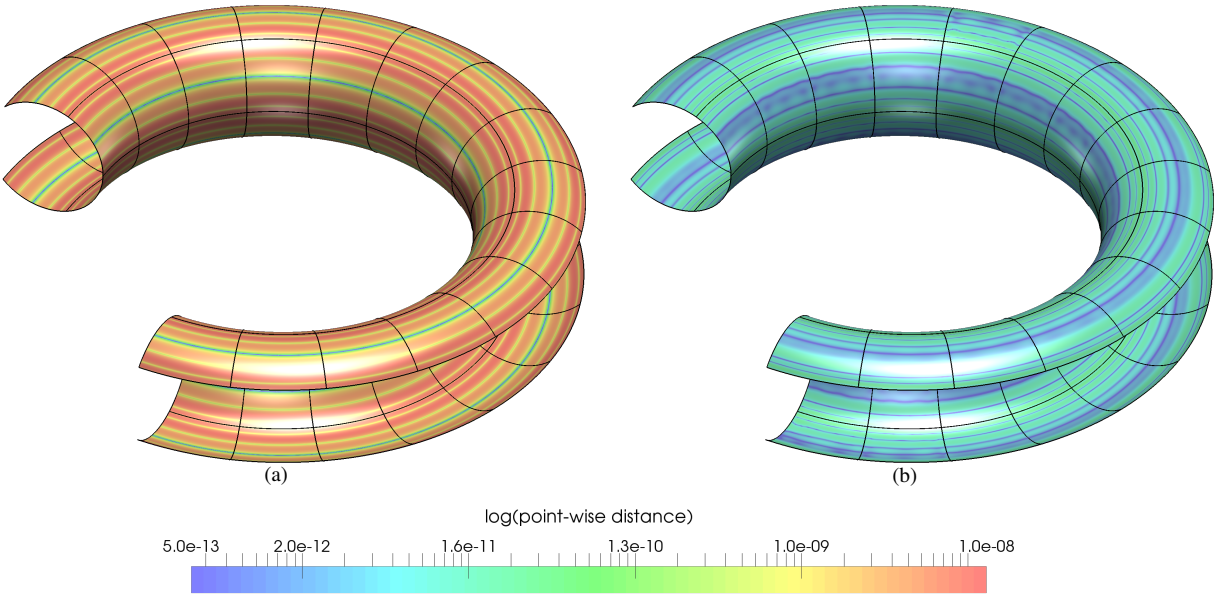

Fig. 8. Mesh of polynomial degree six for the torus. $\mathcal{L}_2$-disparity computed using $q = 8$. (a) Initial interpolating mesh ($d = 7 \cdot 10^{-8}$); and (b) smoothed approximating mesh ($d = 10^{-9}$).

$\mathcal{L}_2$-disparity between the non-interpolative mesh and the manifold is $d\left(\mathcal{M}^0, \Sigma\right) = 10^{-9}$. Note that the $\mathcal{L}_2$-disparity between the manifold and the initial interpolative mesh is almost two orders of magnitude larger than the $\mathcal{L}_2$-disparity between the manifold and the non-interpolative mesh. This example shows that the proposed formulation is able to handle surfaces with non-constant curvature.

4.5. Higher geometric accuracy for the same resolution: NACA0012 airfoil surface

This example shows the surface meshes generated for a NACA0012 airfoil surface. In this example, we generate several meshes with the same resolution. That is, all the meshes contain the same number of nodes, and we change the number of elements and the polynomial degree of each mesh. The objective of this example is to show that the accuracy of the surface representation increases as the polynomial degree increases, even if the resolution of all the meshes is the same. Figure 9 shows the different meshes generated for the NACA0012 airfoil. The left column of Figure 9 shows the initial interpolative meshes for polynomial degrees one, two, four and eight. We have colored the mesh according to the logarithm of the point-wise distance defined in Equation (6). The maximum error of the initial interpolating meshes is located around the leading edge of the profile, because there is the maximum curvature of the geometry. On the contrary, the region around the trailing edge is almost planar and, for this reason, the point-wise distance is lower. The right column shows the corresponding approximating smoothed meshes. Note that the smoothed meshes have higher element density around the leading edge in order to reduce the $\mathcal{L}_2$-disparity. It is important to point out that as the polynomial degree is increased the overall point-wise distance is decreased, even when the resolution of the meshes is kept constant.

Note that there are oscillations of the point-wise distance even in the mesh with highest polynomial degree. The main reason to obtain these oscillations is that the shape of the NACA airfoil surface cannot be represented using the selected piece-wise polynomials. However, it is worth to notice that this oscillations are of the order of $O(10^{-11})$ for the mesh of polynomial degree eight and, for this reason, they are very small compared to the size of the geometry.

Table 1 shows the $\mathcal{L}_2$-disparity of the initial interpolative and the smoothed approximating meshes, against the NACA0012 surface profile, and their corresponding maximum of the point-wise distance. The results of this table are also presented in Figure 10. Note that both the $\mathcal{L}_2$-disparity measure and the maximum of the point-wise distance for the initial meshes are stagnating as the polynomial degree is increased. That is, the deviation between the mesh and

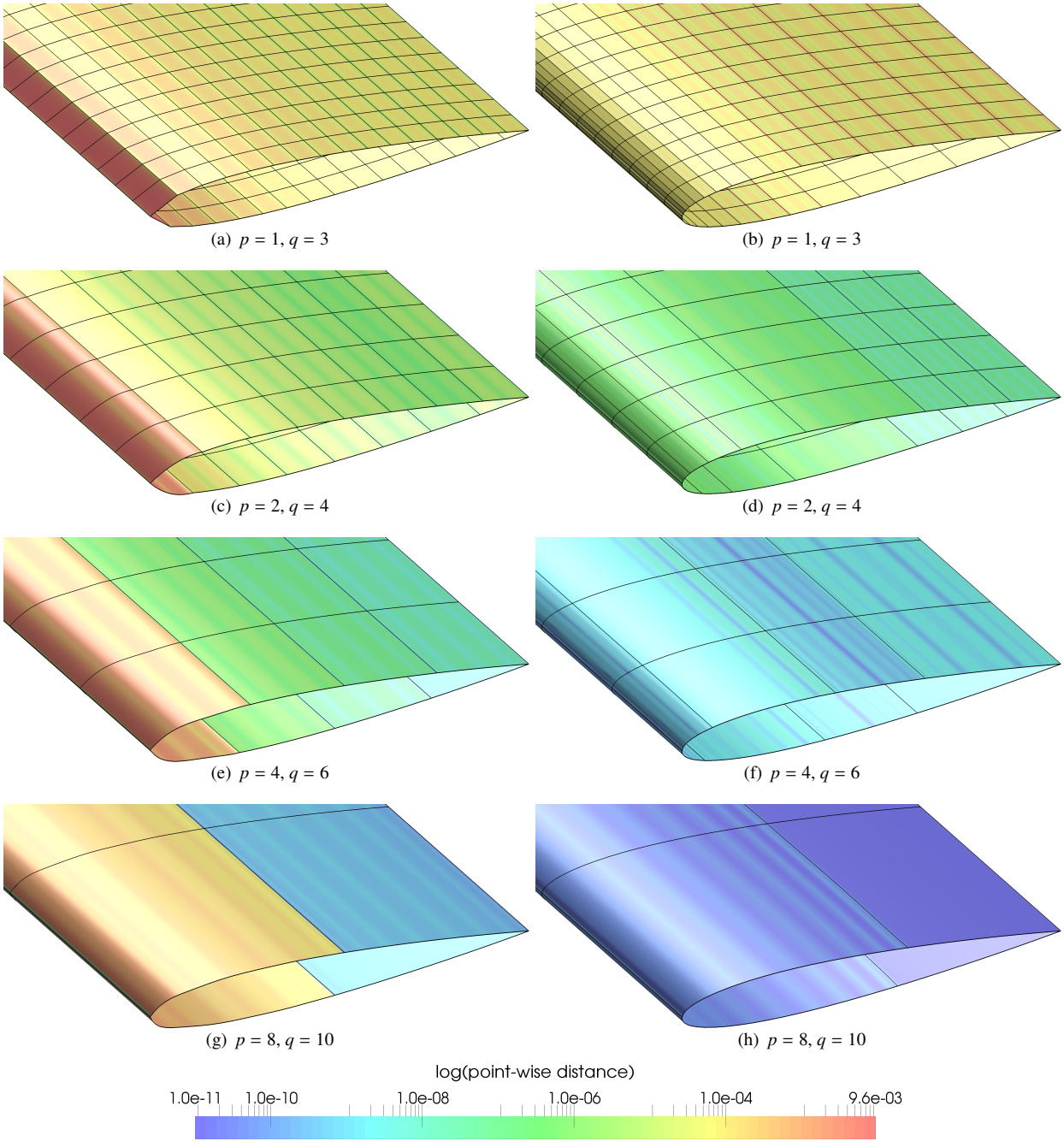

Fig. 9. Meshes generated for the NACA0012 airfoil surface. In columns, initial interpolating meshes (a), (c), (e) and (g); and smoothed approximating meshes (b), (d) , (f) and (h). In rows, the polynomial degrees of the physical and parametric meshes.

the manifold is almost constant. However, the smoothed approximating meshes reduce the $\mathcal{L}_2$-disparity measure and the maximum point-wise distance by orders of magnitude. Even when the resolution of the meshes is kept constant for this example, it is better to increase the interpolating degree of the mesh in order to increase the accuracy of the domain approximation.

Table 1.

	$p = 1$ $h = 0.0625$		$p = 2$ $h = 0.125$		$p = 4$ $h = 0.25$		$p = 8$ $h = 0.5$	
	$\mathcal{L}_2$-disparity	$\sup d(\boldsymbol{\xi})$	$\mathcal{L}_2$-disparity	$\sup d(\boldsymbol{\xi})$	$\mathcal{L}_2$-disparity	$\sup d(\boldsymbol{\xi})$	$\mathcal{L}_2$-disparity	$\sup d(\boldsymbol{\xi})$
initial	$1.1 \cdot 10^{-1}$	$1.5 \cdot 10^{-2}$	$2.9 \cdot 10^{-2}$	$1.1 \cdot 10^{-2}$	$9.9 \cdot 10^{-3}$	$8.1 \cdot 10^{-3}$	$3.1 \cdot 10^{-3}$	$2.8 \cdot 10^{-3}$
smoothed	$3.9 \cdot 10^{-2}$	$9.5 \cdot 10^{-4}$	$1.2 \cdot 10^{-5}$	$2.0 \cdot 10^{-5}$	$2.6 \cdot 10^{-8}$	$9.5 \cdot 10^{-7}$	$3.1 \cdot 10^{-10}$	$2.8 \cdot 10^{-10}$

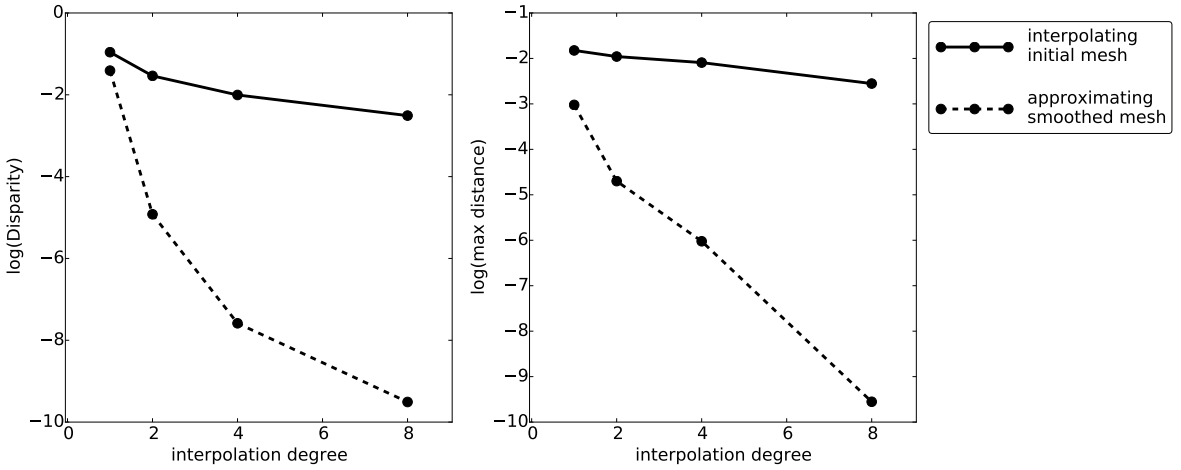

Fig. 10. Polynomial degree against $\mathcal{L}_2$-disparity measure (left); and $\sup d(\boldsymbol{\xi})$ (right).

5. Concluding remarks and future work

In this work we have defined an $\mathcal{L}_2$-disparity measure that computes the deviation between manifolds. The $\mathcal{L}_2$-disparity measure is computed as an infimum of $\mathcal{L}_2$-norm of functions over all the possible orientation-preserving diffeomorphisms between the parametric spaces of the manifolds, $\boldsymbol{\phi}^U$. Note that the proposed disparity is generalizable to manifolds of arbitrary dimension and, for this reason, it can be directly applied to compute the deviations between two curves, or between two surfaces.

We have applied the $\mathcal{L}_2$-disparity measure to compute the deviation between a manifold and its curved high-order approximation. Then, by optimizing the node position of the high-order mesh, we have minimized the $\mathcal{L}_2$-disparity between the mesh and the manifold. To this end, we first approximate the diffeomorphism $\boldsymbol{\phi}^U$ by introducing new unknowns to the minimization problem. Thus, the objective function takes into account the position of the mesh nodes, and the approximation of the diffeomorphism. The proposed objective function is differentiable and therefore, it can be readily used in a minimization process where the first and second derivatives are used. To exploit this, we have used Newton's method combined with a back-tracking line-search procedure.

In the proposed minimization process, we do not impose that the nodes of the mesh are located on the manifold. That is, we do not impose an interpolative high-order mesh. Therefore, the obtained mesh after solving the minimization problem is a non-interpolative high-order mesh. Since we use an $\mathcal{L}_2$ norm, this can be interpreted as a curved high-order mesh that approximates the manifold in a weak sense.

While in this work we have restricted ourselves to use a Lagrangian basis of shape functions, the proposed formulation can handle any combination of element types and shape functions basis. The only requirement of the method is a space of functions provided with an $\mathcal{L}_2$ scalar product. To approximate the integrals coming from the scalar product of functions, a numerical integration rule is also required. Accordingly, any element type that is usually implemented in a solver can be used. Moreover, other kind of shape functions can also be used in the method, even when they are non-interpolative, such as the case of B-spline shape functions.

The proposed method requires a parameterization of the geometric entity to be approximated. While our formulation can deal with any kind of parameterization, in our implementation we have restricted ourselves to CAD

geometries that can be managed by the OpenCASCADE library [17]. In its current state, the formulation and therefore, the implementation, are devised to deal with one entity at a time. Thus, in all the examples presented in this work, we have applied the proposed method to geometries composed of a single untrimmed entity. However, in real case applications, the boundary of the domain is composed of several entities that may be trimmed or not. Thus, we have to extend the proposed formulation in order to handle this kind of geometries. The main idea is to optimize the whole mesh at the same time, even if the elements belong to different entities. Thus, the mesh continuity between different boundary entities will be preserved, as well as the mesh geometric accuracy will be improved.

We have favored to exploit quadratic convergence rates of Newton's method over the reduced memory footprint of node-by-node implementations of smoothing methods. In the near future it could be interesting to compare both approaches in the terms of the computational and memory requirements and the obtained performance. As a reference, we could also compare our formulation with a standard Laplacian smoothing expressed in terms of the parametric coordinates of the nodes. Our formulation has an additional set of design variables that corresponds to the physical coordinates of the curved mesh. Accordingly, the resulting non-linear system has more degrees of freedom (DOFs). Nevertheless, we highlight that the overhead in DOFs of our method pays off in those applications where a mesh of optimal accuracy, *e.g.* convergence studies of numerical methods, is of major importance and cannot be obtained with a standard mesh smoothing method.

This work is not focused on how to create curved volume (planar) meshes that are valid for finite element analysis with unstructured high-order methods. We have addressed this issue in previous works where we propose boundary interpolative curved meshing approaches for planar meshes [18], surface meshes with the nodes on a CAD [19, 20], volume meshes [21], and a one shot approach where the curve, surface and volume nodes are free to slide simultaneously on the boundary entities [22]. In these works, to untangle and smooth a curved high-order mesh we minimize an objective function, E_Q, that measures the mesh distortion [23], while the boundary nodes are either fixed or free to interpolate the domain boundaries. In the near future, we will propose a boundary non-interpolative curved meshing method by freely moving all the nodes of the mesh in the physical space, even the boundary ones. Then, to ensure that the boundary mesh correctly approximates the surfaces (curves) of the geometric model, we will add an additional term that corresponds to the $\mathcal{L}_2$-disparity measure functional presented in this work. That is, we will propose to minimize the functional

$$\widehat{E} = E_Q + E = E_Q + \left\| \boldsymbol{\phi}^P - \boldsymbol{\varphi} \circ \boldsymbol{\phi}^U \right\|^2 .$$

Note that the objective function related with the element quality, E_Q, is defined for the volume (surface) elements, while the objective function related to the $\mathcal{L}_2$-disparity measure, E, is only defined for the surface (curve) elements. By optimizing the new objective function, $\widehat{E}$, we will obtain a high-quality mesh without inverted elements that approximates the boundary surfaces (curves) with optimal convergence rates. It is important to highlight that the first combination of mesh curving with geometry accuracy enhancement have been proposed in [15].

We consider that our method is a relevant alternative to other methods to enhance the geometric accuracy of a curved high-order mesh. Specifically, by considering a non-interpolative method expressed in terms of the physical coordinates and the parametric coordinates of an auxiliary mesh we can reach the optimal convergence rates of the accuracy of the geometric approximation. We have proved in the examples that this convergence property is preserved even for high polynomial degrees, up to degree 8, and independently of the manifold parameterization. Therefore, our method is potentially well suited to generate accurate high-order approximations of non-uniformly parameterized CAD entities that may arise in practical applications. These advantages are of the major usefulness when performing solution convergence studies in the context of unstructured high-order methods. Note that geometrically inaccurate meshes can pollute the approximated solution and therefore, impede to obtain the rates of convergence predicted by the theory. To show the advantages of our method it has been mandatory to code a correct implementation and run the obtained solver with different meshes and target geometries.

Acknowledgements

This research was partially supported by CONACYT-SENER ("Fondo Sectorial CONACYT SENER HIDROCARBUROS", grand contract 163723). The work of the corresponding author was partially supported by the Boeing Co.

& US Air Force Office of Scientific Research & European Comission through the Boeing-MIT Alliance & Computational Math Program & Marie Sklodowska-Curie Actions (HiPerMeGaFlows project), respectively.

References

[1] BA Szabo and I Babuška. *Finite Element Analysis*. John Wiley & Sons New York, 1991.
[2] C Schwab. *p-and hp-finite element methods: Theory and applications in solid and fluid mechanics*. Clarendon Press Oxford, 1998.
[3] MO Deville, PF Fischer, and EH Mund. *High-order methods for incompressible fluid flow*, volume 9. Cambridge University Press, 2002.
[4] JS Hesthaven and T Warburton. *Nodal Discontinuous Galerkin Methods: Algorithms, Analysis, and Applications*. Texts in Applied Mathematics. Springer, 2007.
[5] G Karniadakis and S Sherwin. *Spectral/hp element methods for computational fluid dynamics*. Oxford University Press, 2013.
[6] F Bassi and S Rebay. High-order accurate discontinuous finite element solution of the 2D Euler equations. *Journal of computational physics*, 138(2):251–285, 1997.
[7] S Dey, M Shephard, and JE Flaherty. Geometry representation issues associated with p-version finite element computations. *Comput. Meth. Appl. M.*, 150(1–4):39–55, 1997.
[8] X. Luo, M. S. Shephard, and J.-F. Remacle. The influence of geometric approximation on the accuracy of higher order methods. In *8th International Conference on Numerical Grid Generation in Computational Field Simulations*, 2002.
[9] D Xue and Demkowicz. Control of geometry induced error in *hp* finite element (FE) simulations. I. Evaluation of FE error for curvilinear geometries. *Internat. J. Numer. Anal. Model.*, 2(3):283–300, 2005.
[10] R. Sevilla, S. Fernández-Méndez, and A. Huerta. NURBS–Enhanced Finite Element Method (NEFEM): a seamless bridge between CAD and FEM. *Arch. Comput. Methods Engrg.*, 18(4):441–484, 2011.
[11] A Gargallo-Peiró, X Roca, J Peraire, and J Sarrate. Optimization of a regularized distortion measure to generate curved high-order unstructured tetrahedral meshes. *International Journal for Numerical Methods in Engineering*, 2015.
[12] P Cignoni, C Rocchini, and R Scopigno. Metro: measuring error on simplified surfaces. *Computer Graphics Forum*, 17(2):167–174, 1998.
[13] H Alt and M Godau. Computing the Fréchet distance between two polygonal curves. *International Journal of Computational Geometry & Applications*, 5(1):75–91, 1995.
[14] H Alt and M Buchin. Can we compute the similarity between surfaces? *Discrete & Computational Geometry*, 43(1):78–99, 2010.
[15] JF Remacle, J Lambrechts, C Geuzaine, and T Toulorge. Optimizing the geometrical accuracy of 2D curvilinear meshes. *Procedia Engineering*, 82:228–239, 2014.
[16] J Nocedal and S Wright. *Numerical optimization*. Springer Verlag, 1999.
[17] OpenCASCADE. Open CASCADE Technology, 3D modeling & numerical simulation. `http://www.opencascade.org`, 2013.
[18] X. Roca, A. Gargallo-Peiró, and J. Sarrate. Defining quality measures for high-order planar triangles and curved mesh generation. In *Proc. 20th Int. Meshing Roundtable*, pages 365–383. Springer International Publishing, 2012.
[19] A. Gargallo-Peiró, X. Roca, and J. Sarrate. A surface mesh smoothing and untangling method independent of the CAD parameterization. *Comput. Mech.*, 53(4):587–609, 2014.
[20] A. Gargallo-Peiró, X. Roca, J. Peraire, and J. Sarrate. Defining quality measures for mesh optimization on parameterized CAD surfaces. In *Proc. 21st Int. Meshing Roundtable*, pages 85–102. Springer International Publishing, 2013.
[21] A Gargallo-Peiró, X Roca, J Peraire, and J Sarrate. Optimization of a regularized distortion measure to generate curved high-order unstructured tetrahedral meshes. *Int. J. Numer. Meth. Engng*, (accepted), 2015.
[22] E Ruiz-Gironés, X Roca, and J Sarrate. High-order mesh curving by distortion minimization with boundary nodes free to slide on a 3D CAD representation. *Computer-Aided Design*, DOI: 10.1016/j.cad.2015.06.011, 2015.
[23] A Gargallo-Peiró, X Roca, J Peraire, and J Sarrate. Distortion and quality measures for validating and generating high-order tetrahedral meshes. *Eng Comput*, in press.